RSC Advances

PAPER

View Article Online
View Journal | View Issue

Cite this: *RSC Adv.*, 2021, **11**, 13458

Optical properties and stability of small hollow gold nanoparticles

Ngo T. Dung, *[a] Nguyen T. N. Linh,[b] Dinh L. Chi,[c] Nguyen T. H. Hoa,[b] Nguyen P. Hung,[b] Ngo T. Ha,[b] Pham H. Nam,[d] Nguyen X. Phuc,[d] Le T. Tam [e] and Le T. Lu *[af]

In the current work, small hollow Au nanoparticles ($d \approx 16$ nm) with excellent thermal stability and high photo-thermal conversion efficiency, which have great potential for use in photo-thermal cancer therapy, were prepared through galvanic replacement reaction between Ag nano-templates and gold salt. The position of surface plasmon resonance (SPR) bands for these nanoparticles could be tuned by varying the amount of gold salt. The hydrophobic hollow nanostructures were made water-dispersible by being encapsulated with poly(maleic anhydride-*alt*-1-octadecene) – PMAO. The obtained nanostructures were stable in an aqueous solution of NaCl with concentration up to 280 mM. The hollow gold nanoparticles (HGNPs) were then heated using an 808 nm laser at different power densities, the obtained data showed that they are highly photo-thermal stable under a high power density laser up to 1.6 W cm^{-2} after three circles of irradiation at 20 min per circle (20 min continuous irradiation for each circle). The facile synthesis of small size HGNPs with a plasmon peak in the near infrared range, colloidal and photo-thermal stability, and high capacity of conversion of photon energy into heat makes them a promising material for photo-thermal and imaging applications.

Received 6th November 2020
Accepted 26th March 2021

DOI: 10.1039/d0ra09417j

rsc.li/rsc-advances

1. Introduction

Gold nanostructures have attracted wide interest recently due to their fascinating optical properties known as surface plasmon resonance (SPR) and their diverse application in catalysis,[1–3] sensing,[4–6] photonics[7] and biomedicine.[1,4,8–11] In biomedicine, gold nanostructures with strongly enhanced and tunable optical properties, high biocompatibility, chemical stability and simple surface modification have opened up their practical applications. To date, solid spherical Au nanoparticles having the SPR peak finely tuned between 510 and 600 nm have been extensively studied.[3,12] These spherical Au nanoparticles, however, are less useful in some *in vivo* biomedical applications, for example, photo-thermal cancer therapy, where near-infrared (NIR) light in the range of 650–900 nm is preferred due to its deeper penetration (both blood and soft tissues are highly transparent within this range).[1,8–10]

To overcome the limitation of solid spherical Au nanoparticles, recently, several Au nanostructures, including nanorods, nanoshells (dielectric core/gold shell) and hollow nanostructures which strongly absorb light in the NIR range have been intensively investigated and successfully applied in medicine. For example, Murphy developed gold nanorods with SPR peaks controlled in the range from 600 to 1200 nm by varying the ratio of their length/diameter. Some reports were successful in the control of nanorods by tuning the synthesis conditions.[13–15] However, it was indicated that the nanorods are not thermal stable and in some case, deformed into spherical structures, leading to a large shift of SPR peak from the near-IR region after a short period of irradiation.[16,17] Gold nanoshells with finely tuned optical properties and excellent optical stability, which have great potential for use in photo-thermal cancer therapy, have been developed by Halas *et al.* since the early 2000s.[18] Though, the main disadvantage of Au nanoshells is their relatively large size (usually ≥70 nm). As a result, it is very difficult to sustain them in a solution without precipitation, consequently limiting their practical application. Recently, HGNPs have been attracted special interests for purposes of diagnosis (cancer cell imaging) and therapy (photo-thermal cancer therapy and targeted drug delivery) of cancer, due to their finely tuned SPR peak to the near-infrared region, optical stability and high photo-thermal conversion efficiency.[19] To date, the size of the synthesized HGNPs is still large (30–60 nm).[20–23] In this size range, to disperse and retain the colloidal

[a]*Institute for Tropical Technology, Vietnam Academy of Science and Technology, 18 Hoang Quoc Viet, Hanoi, Vietnam. E-mail: ltlu@itt.vast.vn; ngodunght@gmail.com*
[b]*Thai Nguyen University of Sciences, Tan Thinh Ward, Thai Nguyen City, Vietnam*
[c]*Hanoi-Amsterdam High School for the Gifted, Hoang Minh Giam, Cau Giay, Hanoi, Vietnam*
[d]*Institute of Materials Science, Vietnam Academy of Science and Technology, 18 Hoang Quoc Viet, Hanoi, Vietnam*
[e]*Vinh University, 182 Le Duan Street, Vinh City, Nghe An, Vietnam*
[f]*Graduate University of Science and Technology, Vietnam Academy of Science and Technology, 18 Hoang Quoc Viet, Hanoi, Vietnam*

stability in aqueous solution for a long time is a remaining challenge.

At the present, there are only a few works on the synthesis of small size (≤16 nm) HGNPs.[19,24] Andres *et al.* reported on the synthesis of HGNPs using nanosecond laser irradiation.[24] However, the formation of hollow nanostructures was observed only under certain specific conditions. The absorption peaks of HGNPs are still located in the visible region or small HGNPs were only dispersible in organic solvent,[19] which is not suitable for biomedical applications. The photo-thermal properties of small HGNPs have not been investigated.

In this work, we describe a facile synthesis of small HGNPs (≈16 nm) involved in the galvanic replacement reaction of Ag nanoparticles with gold salt in organic solvent. The hydrophobic HGNPs were then transferred into water by being encapsulated with PMAO. The colloidal stability, optical and photo-thermal properties of the obtained small HGNPs were investigated. The obtained results indicated that the PMAO encapsulated HGNPs were stable in NaCl solution at a concentration up to 280 mM. The SPR peaks shifted from 430 to 700 nm and back to 535 nm as the gold salt solution varied. The optical heating data indicated a high conversion capacity of photo energy into heat and photo-thermal stability of the PMAO encapsulated HGNPs using an 808 nm laser at different power densities or concentration of HGNPs. In addition, they were highly photo-thermal stable under high power density of laser up to 1.6 W cm^{-2} after three circles of irradiation at 20 min per circle.

2. Materials and method

2.1. Chemicals

The chemicals: gold(III) chloride hydrate ($HAuCl_4 \cdot xH_2O$, 99.999%), silver nitrate ($AgNO_3$, 99.9%), oleylamine (OLA) and PMAO were ordered from Sigma-Aldrich, Singapore. The solvents: dichlorobenzene (DCB, 99%), dibenzyl ether (99%), acetone (99.5%), *n*-hexane and chloroform ($CHCl_3$, 99%) were purchased from Acros, USA or Shanghai, China. All chemicals were used as received without any purification.

Gastric cancer cell line AGS (from RIKEN, BRC Cell Engineering Division, Japan); Gibco RPMI 1640 Medium, fetal bovine serum and vancomycin (all from Invitrogen, Cergy-Pontoise, France); DAPI (4′,6-diamidino-2-phenylindole) and MTT reagent (3-(4,5-dimethylthiazol-2-yl)-2,5-diphenyltetrazolium bromide) from Thermo Fisher.

2.2. Synthesis of Ag templates

Silver nanoparticles were synthesized based by the reduction of silver ions in organic solvent at high temperatures. In a typical process, $AgNO_3$ was dissolved in 6 mL OLA. The mixture of $AgNO_3$ in 6 mL OLA was then added into a three-neck flask containing 40 mL DCB. This flask was immersed in an oil bath placed on a heating mantle equipped with a magnetic stirrer. The mixture was refluxed at around 180 °C at a heating rate of 5 °C min^{-1} and maintained for 60 min before cooling down to room temperature. To purify the sample, 15 mL acetone was added into the final reaction solution, the mixture was then centrifugated at 10 000–11 000 rpm for 5 min. The precipitated nanoparticles were re-dispersed in 15 mL *n*-hexane. The purification process was repeated several times to remove all excess free reagents and the collected particles were dispersed in toluene for characterisation.

2.3. Synthesis of hollow Au nanostructures

Hollow gold nanostructures were prepared *via* galvanic replacement method by the reaction of $HAuCl_4$ salt with the prepared Ag nanotemplates. In a typical synthesis, 1 mL solution of the purified Ag sample was diluted into 20 mL dibenzyl ether and stored in the three-neck flask. The solution was magnetically stirred and then slowly heated to the desired temperature. At this temperature, a certain volume of the gold salt solution made of 15 mg $HAuCl_4 \cdot xH_2O$ dissolving in 15 mL dibenzyl ether and 0.5 mL OLA was added into the flask. After 10 min, the solution was cooled down to room temperature. The obtained sample was purified twice as aforementioned before being dispersed in $CHCl_3$.

2.4. Transferring hollow Au nanostructures into water

Hydrophobic hollow gold nanostructures were transferred in water by the encapsulation with PMAO following a recently developed procedure.[23,25,26] In a typical process, a stock solution of PMAO in $CHCl_3$ with a concentration of 10 mg mL^{-1} was prepared. To this solution, 4 mL of chloroform containing 4 mg OLA coated hollow Au NPs was added and sonicated for 1 h. Chloroform was then removed under vacuum, and 4 mL of dilute NaOH solution was added. Then, the solution was sonicated for 10 min and heated at 60 °C for an additional 10 min. Aggregates were removed by centrifugation at 3000 rpm (twice for 15 min), and the excess polymer and NaOH were removed by centrifugation (12 000 rpm for 1 h). The PMAO coated hollow Au nanostructures were finally dispersed in 8 mL water.

2.5. Characterisation

All the TEM images reported in this paper were taken by transmission electron microscope JEM 1010 (JEOL, Japan). Dynamic Light Scattering (DLS) measurements were carried out using a Nanosizer S (Malvern, UK). The optical properties of samples were collected by UV-vis measurements (Jasco V-670, Japan). The photo-thermal effect was investigated on the home-made instrument where the gold sample solution was irradiated with an 808 nm semiconducting laser at different power densities.

The MTT assay was used for the evaluation of the cytotoxicity of HGNPs on gastric cancer cell line AGS. 5×10^3 cells were seeded onto 96-well plates and different concentrations (5, 10, 15, 20, 30 and 40 μg mL^{-1}) of HGNPs were added to the culture media ($n = 5$ for each concentration). Control samples without the addition of the HGNPs were also contained in culture media. After treatment, cells were cultured during the period of 24 hours and 72 hours to evaluate the cell morphology by removing the culture media and adding 100 μL of fresh media containing 20 μL of MTT reagent (5 mg mL^{-1}). After being

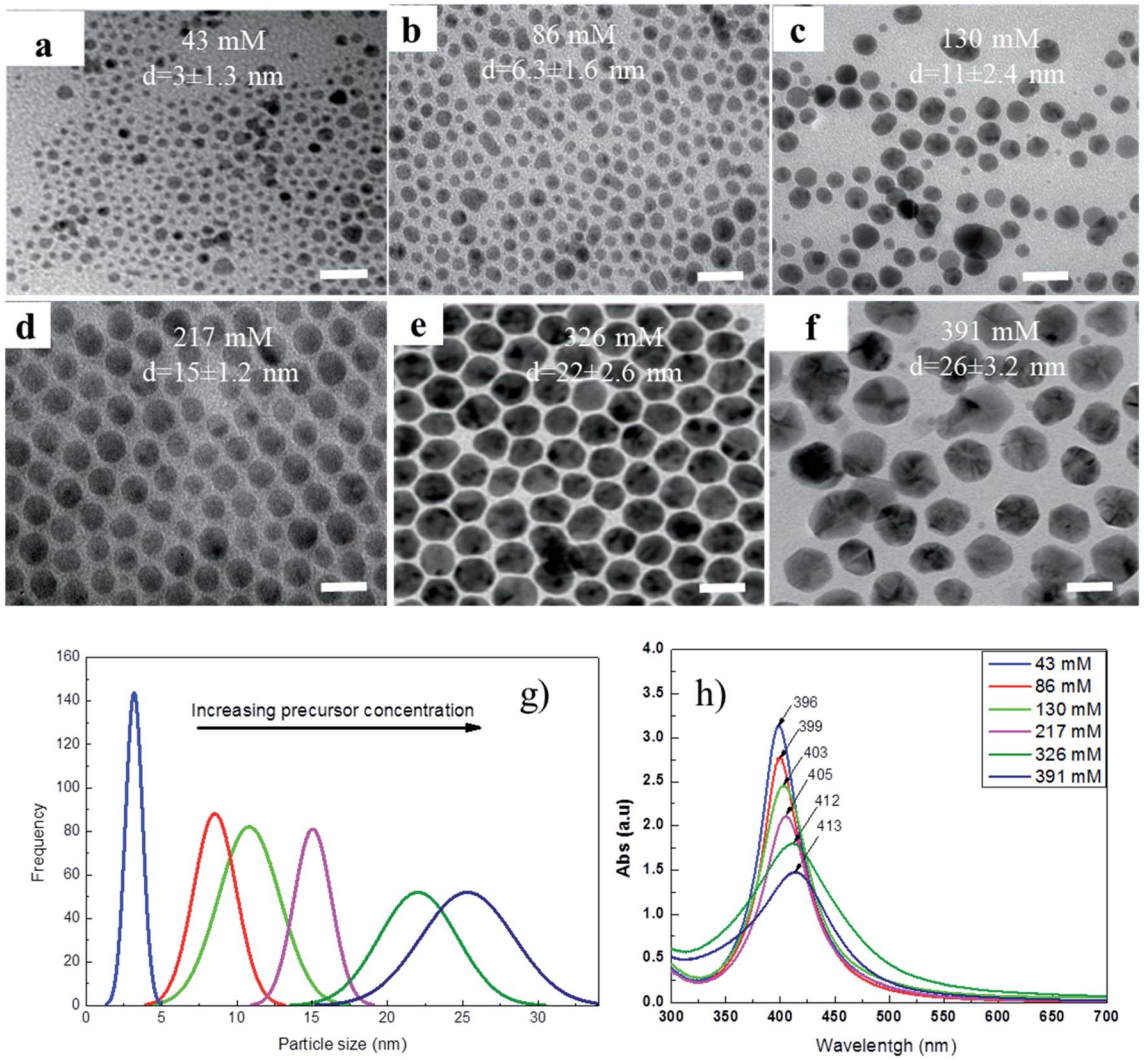

Fig. 1 TEM images of Ag NPs prepared at different Ag precursor concentrations of 43 (a), 86 (b), 130 (c), 217 (d), 326 (e) and 391 mM (f). Size distribution histograms (g) and UV-vis spectra (h) of NPs with different precursor concentrations (43, 86, 130, 217, 326 and 391 mM). Scale bar: 20 nm.

incubated in 5% CO_2 at 37 °C and 95% humidity for 4 h, MTT solution was removed. The samples were added with 100 μL dimethyl sulfoxide (DMSO) and 12 μL of Sorensen buffer (NaCl 0.1 M, glycine 0.1 M adjusted to pH = 10.5 with NaOH 1 M) and then incubated for 15 min at 37 °C. The number of cells was recorded at 570 nm of absorbance using a spectrophotometric plate reader (Multiskan Sky). Cell viability was determined using the formula:

$$\%\ \text{cell viability} = (\text{optical density of sample/optical density of control}) \times 100$$

The influence of HGNPs on AGS cell morphology was controlled as the following procedure: 2×10^6 cells were seeded onto 24-well plates and treated with HGNPs at various concentrations during 72 hours. Cellular morphology was captured using a phase-contrast light microscope (Eclipse Ts2, NIKON).

Nuclear staining with 4′,6-diamidino-2-phenylindole (DAPI) at 1 : 5000 dilution of 10 mg mL^{-1} DAPI. After treatment with or without HGNPs, cells were washed twice with phosphate buffered saline (PBS), permeabilized with 0.5% Triton X for 10 min at room temperature and stained with the DNA-specific fluorochrome DAPI (Invitrogen). Cells washed by PBS and nuclear stained were then observed and recorded fluorescence images using a NIKON Eclipse Ti2U fluorescence microscope (NIKON, Japan).

3. Results and discussions

3.1. Ag templates

It was well known that the optical property of hollow Au nanostructures strongly depends on their morphology which is determined by the morphology of Ag nanoparticles. In our previous work, Ag nanoparticles with different shapes of sphere, cube and rod were synthesized in ethylene glycol (EG) using

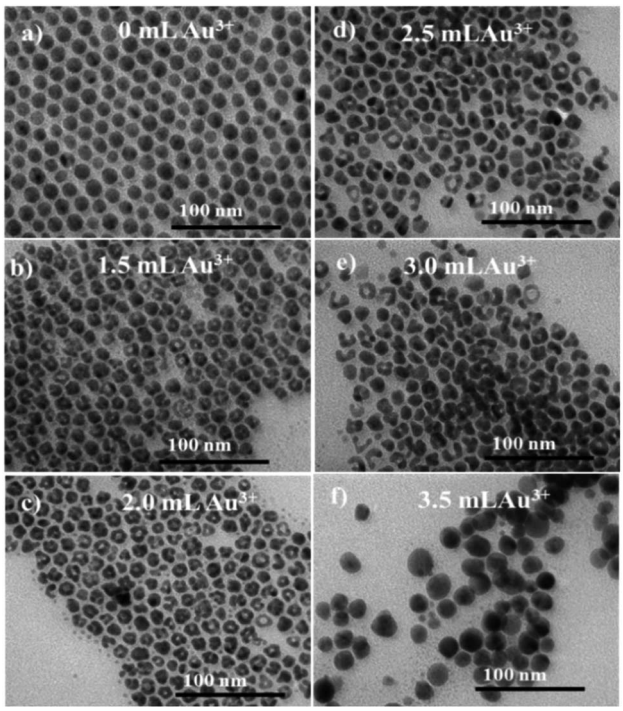

Fig. 2 TEM images of OLA/OA capped Ag templates (a) and hollow Au nanostructure prepared at: 0 mL (a), 1.5 mL (b); 2.0 mL (c), 2.5 (d); 3.0 mL (e) and 3.5 mL $HAuCl_4$ (f). Scale bar: 100 nm.

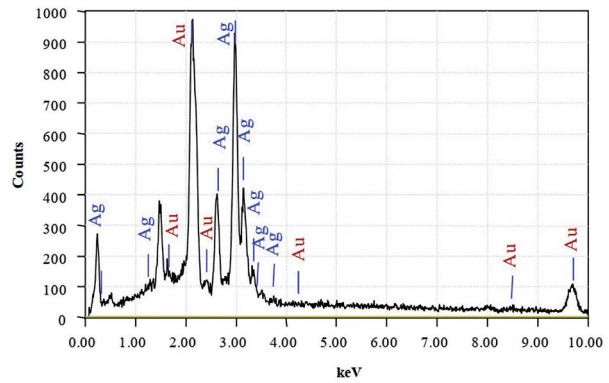

Fig. 3 EDS spectra of hollow Au nanostructure prepared at 3.0 mL $HAuCl_4$ solution.

poly(vinylpyrrolidone) (PVP) as a capping ligand.[23] However, these nanoparticles are relatively large (40–100 nm) and thus were readily precipitated in solution. In the current work, with an attempt to reduce the particle size of Ag NPs, we replaced EG by DCB and PVP was replaced by OLA, a stronger reductive reagent.

Fig. 1 shows TEM images of the Ag nanoparticles synthesized at various concentrations of $AgNO_3$ precursor. It can be seen that the morphology of Ag NPs has no significant change in all cases, the spherical Ag NPs with the mean size from 3 to 26 nm were observed when the concentrations of $AgNO_3$ precursor varied from 43 to 391 mM, correspondingly. This change in the particle size can be seen more clearly in Fig. 1g. In addition, the UV-vis spectra of the samples (Fig. 1h) also show that the surface plasmon resonance (SPR) peak shifts from 396 to 413 nm corresponding to the change in the particle size.

3.2. Au hollow structures

Hollow Au nanostructures were formed *via* the galvanic replacement reaction using Ag NPs as nano-templates. The chemical reaction involved in the galvanic replacement process is as follows:

$$3Ag^0\,(s) + Au^{3+} = Au^0\,(s) + 3Ag^+$$

Herein, the Ag NPs serve as both reducing agent and nano-template to form the hollow Au nanostructures. The Ag sample synthesized at 217 mM $AgNO_3$ precursor (Fig. 1d) with a size of 15 nm was used as nanotemplate for the formation of the hollow gold nanoparticles. Fig. 2 shows TEM images of Ag templates (0 mL $HAuCl_4$ solution) and Au nanostructures prepared at the different volumes of $HAuCl_4$ solution. From the TEM images, it can be seen that the obtained Au NPs are hollow nanostructures when the volumes of $HAuCl_4$ solution varied in the range of 1.5 to 3.0 mL. The formation of Au hollow nanostructures was evidenced by the darker at the edge than inside of the particles on the TEM images due to the mass contrast. The hollow Au nanostructure was further confirmed by the changes of the optical property and colour of solution (Fig. 5) and will be discussed in the following section. As the volume of $HAuCl_4$ increased to 3.5 mL, the hollow nanostructures gradually broke down to form solid NPs.

The chemical composition of the hollow Au nanostructure synthesized with 2.0 mL $HAuCl_4$ was determined through energy dispersive X-ray spectroscopy (EDS) (Fig. 3). The results show that the hollow Au nanostructure has characteristic peaks of the main elements including Ag and Au. In addition, the presence of low-intensity peaks of C and N is due to the contribution of surfactants. The chemical composition of the hollow Au samples synthesized at different volumes of gold salts is detailed in Table 1. As we can see, the composition of Au elements increases as the amount of gold salts increases. The increase in Au content corresponds to the reduction of Ag

Table 1 The atomic composition of hollow Au nanostructure prepared at different volumes of $HAuCl_4$

The volume of $H[AuCl_4]$ (mL)	Weight (%)			
	Ag	Au	C	N
0	94.78	0	3.47	1.54
0.5	90.18	5.01	3.36	1.45
1.0	82.95	11.16	3.58	2.15
1.5	77.64	17.30	3.52	1.42
2.0	69.22	25.77	3.47	1.54
2.5	58.75	36.11	3.32	1.56
3.0	48.16	47.38	3.14	1.32
3.5	36.25	58.05	3.25	2.16

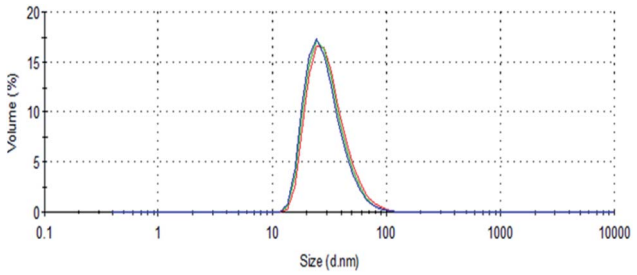

Fig. 4 DLS spectra of PMAO coated hollow Au nanostructure in water under different NaCl concentrations: 200 mM (blue), 250 mM (green) and 280 mM (red).

component, indicating the substitution of gold for silver *via* galvanic replacement process to form a hollow structure (Fig. 2).

3.3. Colloidal stability of hollow Au nanostructures in aqueous solution

For biomedical applications, the hollow Au nanostructures have to be aqueous dispersible and colloidally stable in the solution. In our previous work, we successful used PMAO to transfer a variety of magnetic nanoparticles from organic solvent into water.[25–27] The PMAO encapsulated NPs were then utilized to evaluate the MRI contrast and magnetic induced heating effects.

In the current study, we use a similar approach to coat hollow Au NPs. After transferring into water, PMAO encapsulated Au NPs are well dispersed and stable in water for at least 6 months and under different pH values or NaCl concentrations. Fig. 4 shows DLS spectra of PMAO encapsulated hollow Au nanostructures under different NaCl concentrations of 200, 250 and 280 mM. As for the NaCl concentrations up to 280 mM, the hydrodynamic size remained almost unchanged at around 26 nm, indicating that PMAO capped Au nanostructures did not aggregate but remain well disperse and stable in solution.

3.4. Optical properties

The optical property of the samples was recorded using UV-vis measurements. Fig. 5 shows the UV-vis spectra of the samples prepared at different volumes of $HAuCl_4$ solution. It is evident that the plasmon resonance of the NPs depends strongly on the amount of Au^{3+} salt solution added. The 15 nm Ag nanotemplate solution (0 mL $HAuCl_4$) exhibited a typically narrow and strong SPR peak of solid Ag NPs at around 400 nm. When a small volume of Au^{3+} salt solution (0.5 mL) was added, the absorption spectrum of the sample appeared two peaks at 430 and 550 nm. The peak at 430 nm is assigned to Ag nanotemplates and the other is stem of the Au shell.

Further adding the $HAuCl_4$ solution, the SPR peak of the samples was possible tuned finely to the NIR region. For example, at 1.0 mL $HAuCl_4$ solution, Ag/Au NPs solution exhibited a SPR peak of 612 nm. The sample shows a broad plasmonic absorption peak from 600 to 850 nm with a maximum at around 700 nm when the $HAuCl_4$ solution increases to 2.0 mL. The red-shift of the absorption peak to NIR

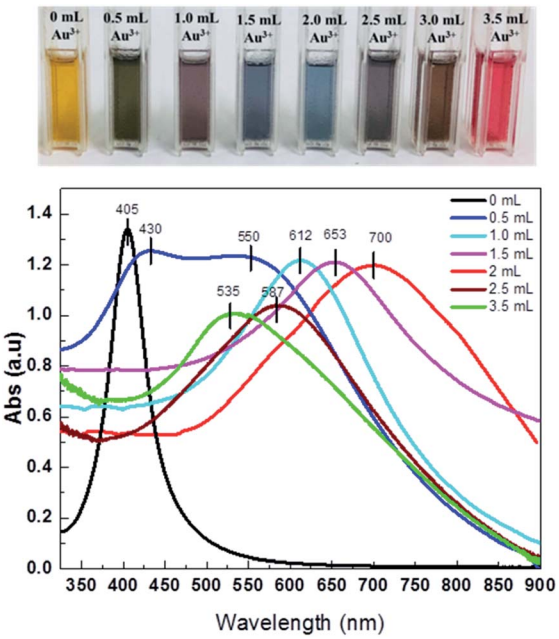

Fig. 5 UV-vis spectra of hollow gold samples synthesized with different volumes of $HAuCl_4$ solution (0, 0.5, 1.0, 1.5, 2.0, 2.5 and 3.5 mL) and the corresponding photos of their solution.

region of the hollow Ag/Au NPs with the increase of Au^{3+} salt solution used is due to the increasing voids as observed in Fig. 2. This was previously reported for hollow Au nanocubes.[23] In the current study, when the Au^{3+} salt solution continuously increases to 2.5 and 3.5 mL, a blue-shift of the SPR peak from 700 for 2.0 mL Au^{3+} salt solution to 587 (2.5 mL) and 535 nm (3.5 mL) was observed. The blue-shift of the SPR peak of the sample at high volumes of $HAuCl_4$ solution is explained by the breaking down of the hollow Au NPs to form solid Au NPs (Fig. 2f). The change in the absorption peaks was visually observed by the change in the colour of Au solutions, as seen in Fig. 5.

3.5. *In vitro* cytotoxic results

In the current study, the hollow Au NPs prepared at 2.0 mL $HAuCl_4$ solution were evaluated cytotoxicity and photo-thermal conversion efficiency. After 24 h of treatment by the hollow Au NPs at different concentrations, there was no significant difference in cell growth, implying the negligible influence of these particles. The cytotoxic effects of the HGNPs were estimated in terms of growth inhibition percentage that did not exceed 20% compared to the control. In contrast, the inhibitory effect of nanoparticles on cell proliferation was significantly increased after 72 h of treatment at high concentration from 20–40 $\mu g\ mL^{-1}$. However, there were no obvious differences in the cell morphology at the whole concentration range of the NPs (Fig. 6).

Previous studies have verified that gold is relatively safe both *in vitro* and *in vivo* because it is less likely to be ionized than other metals.[28] Our previous experiments showed that the PMAO coating was biocompatible.[27] Therefore, the toxicity of the HGNPs on AGS cells can be attributed to the following

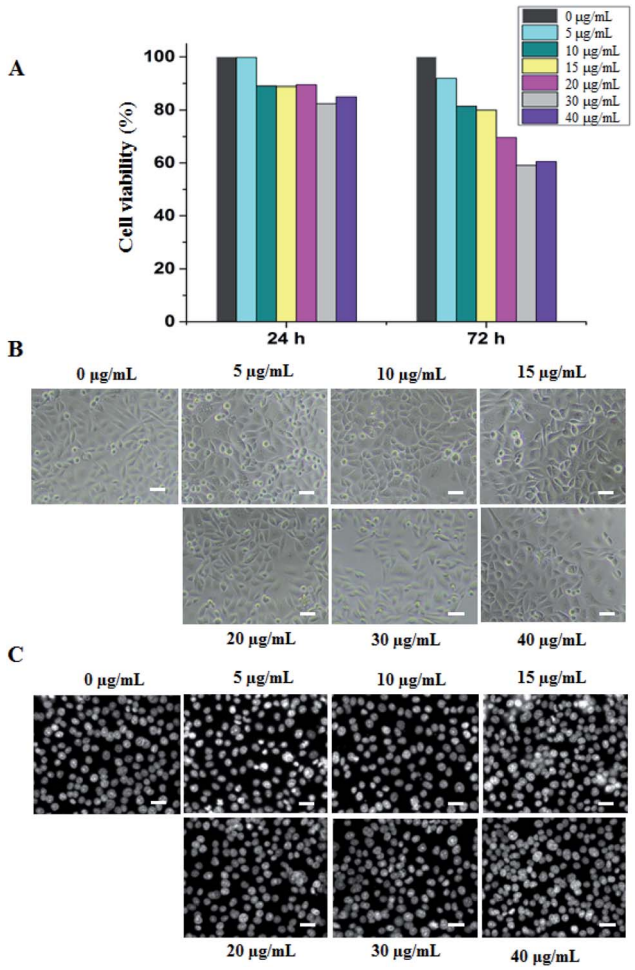

Fig. 6 The effect of HGNPs on cellular proliferation (A). Representative images of cellular morphology of AGS cells after 72 h of treatment, compared to the control (0 μg mL^{-1}) (B). Nuclear morphology in cells was stained or unstained with DAPI at various concentrations of HGNPs after 72 h (C). Scale bars: 50 μm.

reasons: (1) the HGNPs contain a large amount of Ag (69.22% weight, Table 1), (2) the HGNPs have hollow nanostructure so that the association between the PMAO coating and the material surface is restricted. When the cationic silver (Ag^+) is easily released from the hollow structure, the Ag^+ ions might bind to the phospholipid bilayer (the component of cell membrane), subsequently caused changes in its permeability by oxidation reaction and causing apoptosis.[29] The more time to be treated, the more Ag^+ ions in the cell membrane block the uptake of nutrition in the culture media. This is the reason why after 72 h of treatment, the proliferated rate decreased significantly. The same explanation for the higher concentrations of HGNPs is shown in Fig. 6A. Furthermore, the disruption in mitochondria function may occur if Ag^+ ions go through the membrane into the cell by diffusion or endocytosis mechanism, inducing reactive oxygen species (ROS) which are damaging to proteins and nucleic acids including both RNA and DNA, hence the results is the inhibition of cell proliferation.[30–32]

3.6. Photo-thermal effect of hollow Au nanostructures

We investigated the photo-thermal effect and thermal stability of PMAO encapsulated hollow Au NPs under the NIR laser irradiation. The heating was conducted by irradiating around 0.2 mL hollow Au colloidal solution with an 808 nm diode laser at power density up to 1.6 W cm^{-2}. During the NIR absorption process, the absorbed energy by HGNPs will be transferred into thermal energy, consequently heating up the surroundings. The changes in temperature of HGNPs solutions with irradiation time and power density at various current of laser and different concentrations of the HGNPs were recorded by the computer; the data was presented in Fig. 7. Clearly, the temperatures of the aqueous solutions containing hollow Au NPs (at 40 μg mL^{-1})

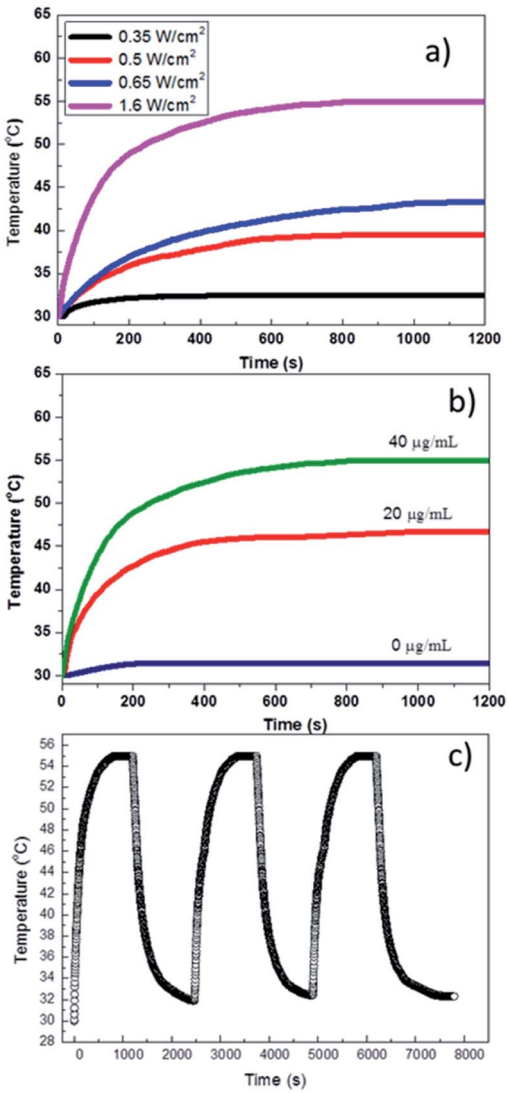

Fig. 7 (a) The temperature change with the irradiation time of hollow Au colloidal solution (40 μg mL^{-1} concentration) under different power densities of the laser in the range from 0.35 to 1.6 W cm^{-2}. (b) The temperature change with different concentrations of Au under 808 nm laser irradiation at the power density of 1.6 W cm^{-2}. (c) The stable photo-thermal conversion after three times irradiation under high power density of laser up to 1.6 W cm^{-2}.

increased with the irradiation time at the power density of 0.35 to 1.6 W cm^{-2}. When the power density remains at 1.6 W cm^{-2}, the increase rate was proportional to the concentration of the NPs. For the lowest power density of 0.35 W cm^{-2}, a small change in the temperature from 30 to 32.5 °C was recorded after 10 min of irradiation. At the intermediate power densities in the range from 0.5 to 0.65 W cm^{-2}, the highest temperature of the sample varied from 37.5 to 43 °C. Under the maximum laser power density of 1.6 W cm^{-2}, the solution temperature reached 50 °C after just 200 seconds and quickly reached the saturation value of around 55 °C (Fig. 7a). At the different Au concentrations of 0, 20 and 40 μg mL^{-1}, the saturation temperatures of the samples were 31.4, 46.7 and 55 °C (Fig. 7b). Pure water sample (0 μg mL^{-1} of Au) showed only an insignificant temperature increase (1.4 °C), indicating that the temperature increase of the samples was due to the heating effect of the PMAO encapsulated hollow Au NPs. This high temperature suggests a high capacity of photo-thermal conversion during the heating.

Hollow Au colloidal solution was irradiated continuously for about 20 min, then the laser source turned off, after the sample temperature dropped to room temperature, the laser source restarted. This process was repeated 3 times with a total irradiation time of 60 min and the results are shown in Fig. 7c. It can be seen that the variation in sample temperature over time is a stable process without any attenuation between different projection cycles. This suggested that thermal and colloidal stability of the nanoparticles is not affected by laser irradiation.

The successfulness in the fabrication of the small hollow Au nanostructures having SPR peak in NIR region and high capacity of conversion of photo energy into heat, photothermal and colloidal stabilities made them become a promising material for therapy and photo imaging applications.

4. Conclusions

Small hollow Au nanostructures (≈16 nm) were fabricated utilizing Ag nanoparticles as self-sacrificed nanotemplates. The size and uniformity of Ag nanotemplates were well controlled by varying the concentration of $AgNO_3$ precursor. The obtained hollow Au NPs showed a red-shift of the SPR peak to 700 nm and exhibited a high capacity of photo-thermal conversion. It also revealed that hollow Au NPs are promising for applications in bio-imaging, photo-thermal therapy and controlled drug release.

Conflicts of interest

There are no conflicts to declare.

Acknowledgements

This research is funded by Vietnam National Foundation for Science and Technology Development (NAFOSTED) under grant number 103.02-2017.334. NXPhuc, LTLu and PHNam thank the AOARD under FA2386-17-1-4042 for financial support.

References

1 R. Ojani, R. Valiollahi and J. B. Raoof, Au hollow nanospheres on graphene support as catalyst for sodium borohydride electrooxidation, *Appl. Surf. Sci.*, 2014, **311**, 245–251.
2 C. W. Yen, M. A. Mahmoud and M. A. El-Sayed, Photocatalysis in gold nanocage nanoreactors, *J. Phys. Chem. A*, 2009, **113**, 4340–4345.
3 P. Suchomel, *et al.*, Simple size-controlled synthesis of Au nanoparticles and their size-dependent catalytic activity, *Sci. Rep.*, 2018, **8**, 1–11.
4 J. Cao, T. Sun and K. T. V. Grattan, Gold nanorod-based localized surface plasmon resonance biosensors: a review, *Sens. Actuators, B*, 2014, **195**, 332–351.
5 S. Liu, J. Liu, X. Han, Y. Cui and W. Wang, Electrochemical DNA biosensor fabrication with hollow gold nanospheres modified electrode and its enhancement in DNA immobilization and hybridization, *Biosens. Bioelectron.*, 2010, **25**, 1640–1645.
6 S. Guo and E. Wang, Noble metal nanomaterials: controllable synthesis and application in fuel cells and analytical sensors, *Nano Today*, 2011, **6**, 240–264.
7 X. Yang, S. E. Skrabalak, Z. Y. Li, Y. Xia and L. V. Wang, Photoacoustic tomography of a rat cerebral cortex in vivo with Au nanocages as an optical contrast agent, *Nano Lett.*, 2007, **7**, 3798–3802.
8 D. Kim and S. Jon, Gold nanoparticles in image-guided cancer therapy, *Inorg. Chim. Acta*, 2012, **393**, 154–164.
9 C. S. Kim, G. Y. Tonga, D. Solfiell and V. M. Rotello, Inorganic nanosystems for therapeutic delivery: status and prospects, *Adv. Drug Delivery Rev.*, 2013, **65**, 93–99.
10 B. G. Prevo, S. A. Esakoff, A. Mikhailovsky and J. A. Zasadzinski, Scalable routes to gold nanoshells with tunable sizes and response to near-infrared pulsed-laser irradiation, *Small*, 2008, **4**, 1183–1195.
11 E. B. Dickerson, *et al.*, Gold nanorod assisted near-infrared plasmonic photothermal therapy (PPTT) of squamous cell carcinoma in mice, *Cancer Lett.*, 2008, **269**, 57–66.
12 S. Ma, *et al.*, Controlled growth of CdS-$Cu_{2-x}S$ lateral heteroshells on Au nanoparticles with improved photocatalytic activity and photothermal efficiency, *J. Mater. Chem. A*, 2019, **7**, 3408–3414.
13 M. R. K. Ali, B. Snyder and M. A. El-Sayed, Synthesis and optical properties of small Au nanorods using a seedless growth technique, *Langmuir*, 2012, **28**, 9807–9815.
14 H. Jia, C. Fang, X. M. Zhu, Q. Ruan, Y. X. J. Wang and J. Wang, Synthesis of absorption-dominant small gold nanorods and their plasmonic properties, *Langmuir*, 2015, **31**, 7418–7426.
15 Z. S. Mbalaha, P. R. Edwards, D. J. S. Birch and Y. Chen, Synthesis of small gold nanorods and their subsequent functionalization with hairpin single stranded DNA, *ACS Omega*, 2019, **4**, 13740–13746.

16 C. C. Chen, *et al.*, DNA-gold nanorod conjugates for remote control of localized gene expression by near infrared irradiation, *J. Am. Chem. Soc.*, 2006, **128**, 3709–3715.
17 W. Albrecht, T. S. Deng, B. Goris, M. A. V. Huis, S. Bals and A. V. Blaaderen, Single particle deformation and analysis of silica coated gold nanorods before and after femtosecond laser pulse excitation, *Nano Lett.*, 2016, **16**, 1818–1825.
18 S. R. Sershen, S. L. Westcott, N. J. Halas and J. L. West, Temperature-sensitive polymer-nanoshell composites for photothermally modulated drug delivery, *J. Biomed. Mater. Res.*, 2000, **51**, 293–298.
19 Y. Yin, C. Erdonmez, S. Aloni and A. P. Alivisatos, Faceting of nanocrystals during chemical transformation: from solid silver spheres to hollow gold octahedra, *J. Am. Chem. Soc.*, 2006, **128**, 12671–12673.
20 R. Wang, J. Deng, D. He, E. Yang, W. Yang, D. Shi, Y. Jiang, Z. Qiu, T. J. Webster and Y. Shen, PEGylated hollow gold nanoparticles for combined X-ray radiation and photothermal therapy in vitro and enhanced CT imaging in vivo, *Nanomedicine*, 2019, **16**, 195–205.
21 J. Depciuch, M. Stec, A. Maximenko, J. Baran and M. P. Wojtan, Temperature-controlled synthesis of hollow, porous gold nanoparticles with wide range light absorption, *J. Mater. Sci.*, 2020, **55**, 5257–5267.
22 Y. Li, D. He, J. Tu, R. Wang, C. Zu, Y. Chen, W. Yang, D. Shi, T. J. Webster and Y. Shen, Comparative effect of wrapping solid gold nanoparticles and hollow gold nanoparticles with doxorubicin-loaded thermosensitive liposomes for cancer thermo-chemotherapy, *Nanoscale*, 2018, **10**, 8628–8641.
23 N. T. Dung, *et al.*, Hollow gold nanostructures prepared by galvanic replacement reaction: synthesis and optical properties, *J. Sci. Technol.*, 2015, **53**, 796.
24 G. G. Rubio, T. M. de Oliveira, W. Albrecht, P. D. Nunez, J. C. Castro-Palacio, A. Prada, R. I. Gonzalez, L. Scarabelli, L. Banares, A. Rivera, L. M. L. Marzan, O. P. Rodriguez, S. Bals and G. M. Andres, Formation of hollow gold nanocrystals by nanosecond laser irradiation, *J. Phys. Chem. Lett.*, 2020, **11**, 670–677.
25 N. T. Dung, *et al.*, High magnetisation, monodisperse and water-dispersible CoFe@Pt core/shell nanoparticles, *Nanoscale*, 2017, **9**, 8952–8961.
26 V. T. K. Oanh, L. T. Tam, D. H. Doan, N. X. Truong, N. X. Ca, V. T. Thu, L. T. Lu and T. D. Lam, PMAO-assisted thermal decomposition synthesis of high-stability ferrofluid based on magnetite nanoparticles for hyperthermia and MRI applications, *Mater. Chem. Phys.*, 2020, **245**, 122762.
27 P. H. Nam, L. T. Lu, P. H. Linh, D. H. Manh, L. T. T. Tam, N. X. Phuc, P. T. Phong and I. J. Lee, Polymer-coated cobalt ferrite nanoparticles: synthesis, characterization, and toxicity for hyperthermia applications, *New J. Chem.*, 2018, **42**, 14530–14541.
28 M. S. Kang, S. Y. Lee, K. S. Kim and D. W. Han, State of the art biocompatible gold nanoparticles for cancer theragnosis, *Pharmaceutics*, 2020, **12**, 701–722.
29 D. McShan, P. C. Ray and H. Yu, Molecular toxicity mechanism of nanosilver, *J. Food Drug Anal.*, 2014, **22**, 116–127.
30 A. C. Burdusel, O. Gherasim, A. M. Grumezescu, L. Mogoanta, A. Ficai and E. Andronescu, Biomedical applications of silver nanoparticles: an up-to-date overview, *Nanomaterials*, 2018, **8**, 681–705.
31 A. Haase, *et al.*, Effects of silver nanoparticles on primary mixed neural cell cultures: uptake, oxidative stress and acute calcium responses, *Toxicol. Sci.*, 2012, **126**, 457–468.
32 E. Zielinska, A. Zauszkiewicz-Pawlak, M. Wojcik and I. Inkielewicz-Stepniak, Silver nanoparticles of different sizes induce a mixed type of programmed cell death in human pancreatic ductal adenocarcinoma, *Oncotarget*, 2018, **9**, 4675–4697.